Half-Sandwich Group 4 Salicyloxazoline Catalysts

Stuart R. Coles,† Guy J. Clarkson,† Andrew L. Gott,† Ian J. Munslow,†
Stefan K. Spitzmesser,‡ and Peter Scott*,†

Department of Chemistry, University of Warwick, Coventry CV4 7AL, U.K., and INEOS Technologies, Rue de Ransbeek 310, 1120 Brussels, Belgium

Received July 31, 2006

A new class of zirconium and hafnium half-sandwich complexes bearing Cp* and salicyloxazolinato (L) ligands has been prepared by salt elimination and protonolysis routes. The analogous Cp and indenyl compounds are generally inaccessible, as are the titanium compounds. The molecular structures of four examples [Cp*MLX_2] (variously M = Zr, Hf; X = Cl, Me) reveal chiral-at-metal structures which persist in solution, according to variable-temperature NMR studies; $\Delta G^{\ddagger}_{298}$ for the racemization process was found to be ca. 75 kJ mol^{-1}. Treatment of these compounds with MAO, $[Ph_3C][B(C_6F_5)_4]$, or $[PhNMe_2H][B(C_6F_5)_4]$ leads to catalysts for alkene polymerization, the nature of which depends on the cocatalyst chosen. The anilinium salt smoothly produces a single chiral species, [Cp*ZrLMe][$B(C_6F_5)_4$], detected also by ^{1}H NMR spectroscopy, which is a highly active single-site catalyst for polymerization of ethene (and less active for copolymerization of ethene/hexene). The trityl activator produces the same catalyst and at least one other catalytically competent species, as evidenced by NMR spectroscopy and polymer modality. The use of MAO leads to a less well-defined catalyst system. The steric demand of the salicyloxazoline ligand affects the catalyst performance significantly, and computational studies show that access of ethene to either of two inequivalent coordination sites is restricted. This stability of the species [Cp*ZrLMe]$^+$ with respect to addition appears to be the limiting factor for catalytic activity. Catalyst stability is addressed, and the steric and electronic factors affecting this are consistent with a mechanism of catalyst death by salicyloxazoline ligand loss.

Introduction

The mechanism of alkene polymerization by group 4 metallocene catalysts of the type Cp_2MX_2 is now quite well understood.[1] In conjunction with cocatalysts such as methylaluminoxane (MAO),[2] the species [CpMR]$^+$ are formed which contain a vacant coordination site cis to the growing polymer chain R, where the monomer alkene may bind as a precursor to the 1,2-migratory insertion (propagation) process. Alternative supporting ligand sets to the various cyclopentadienyls have been studied intensively.[3] Of particular relevance here are the complexes [$(PI)_2MX_2$] (PI = phenoxy-imine (**I**)) developed by Fujita[4] and Coates.[5] A number of hybrid precatalysts containing one cyclopentadienyl ring and one monoanionic bidentate ligand have also been developed, including the amidinates, e.g., **II**,[6] and pyridyl-alkoxides, e.g., **III**.[7] Recently, Bochmann explored a range of phenoxy-imine, e.g., [CpM(PI)Cl_2] (**IV**) and related catalysts, noting that these inherently chiral systems may allow stereoselective polymerization of α-olefins.[8] Unfortunately, however, multimodal polymers were produced, indicating the presence of several catalytically active species, an issue which

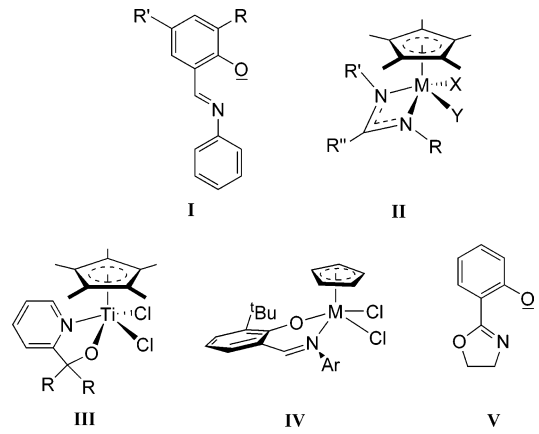

* To whom correspondence should be addressed. E-mail: peter.scott@warwick.ac.uk. Fax: 024 7657 2710.
† University of Warwick.
‡ INEOS Technologies.

(1) (a) Jordan, R. F. *Adv. Organomet. Chem.* **1991**, *32*, 325. (b) Britzinger, H. H.; Fischer, D.; Mulhaupt, R.; Rieger, B.; Waymouth, R. *Angew. Chem., Int. Ed.* **1995**, *34*, 1143. (c) Bochmann, M. *J. Chem. Soc., Dalton Trans.* **1996**, 255. (d) Chen, E. Y. X.; Marks, T. J. *Chem. Rev.* **2000**, *100*, 1391. (e) Resconi, L.; Cavallo, L.; Fait, A.; Piemontesi, F. *Chem. Rev.* **2000**, *100*, 1253. (f) Sillars, D. R.; Landis, C. R. *J. Am. Chem. Soc.* **2003**, *125*, 9894. (g) Liu, Z.; Somsook, E.; White, C. B.; Rosaaen, K. A.; Landis, C. R. *J. Am. Chem. Soc.* **2001**, *123*, 11193.

(2) (a) Bryant, P. L.; Harwell, C. R.; Mrse, A. A.; Emery, E. F.; Gan, Z.; Caldwell, T.; Reyes, A. P.; Kuhns, P.; Hoyt, D. W.; Simeral, L. S.; Hall, R. W.; Butler, L. G. *J. Am. Chem. Soc.* **2001**, *123*, 12009. (b) Zurek, E.; Ziegler, T. *Prog. Polym. Sci.* **2004**, *29*, 107. (c) Zakharov, V. A.; Talzi, E. P.; Zakharov, I. I.; Babushkin, D. E.; Semikolenova, N. V. *Kinet. Catal.* **1999**, *40*, 836.

(3) (a) Gibson, V. C.; Spitzmesser, S. K. *Chem. Rev.* **2003**, *103*, 283. (b) Britovsek, G. J. P.; Gibson, V. C.; Wass, D. F. *Angew. Chem., Int. Ed.* **1999**, *38*, 428. (c) Ittel, S. D.; Johnson, L. K.; Brookhart, M. *Chem. Rev.* **2000**, *100*, 1169.

(4) (a) Furuyama, R.; Saito, J.; Ishii, S.; Makio, H.; Mitani, M.; Tanaka, H.; Fujita, T. *J. Organomet. Chem.* **2005**, *690*, 4398. (b) Makio, H.; Fujita, T. *Bull. Chem. Soc. Jpn.* **2005**, *78*, 52. (c) Mitani, M.; Saito, J.; Ishii, S.-I.; Nakayama, Y.; Makio, H.; Matsukawa, N.; Matsui, S.; Mohri, J.-I.; Furuyama, R.; Terao, H.; Bando, H.; Tanaka, H.; Fujita, T. *Chem. Rec.* **2004**, *4*, 137. (d) Suzuki, Y.; Terao, H.; Fujita, T. *Bull. Chem. Soc. Jpn.* **2003**, *76*, 1493. (e) Makio, H.; Kashiwa, N.; Fujita, T. *Adv. Synth. Catal.* **2002**, *344*, 477.

10.1021/om060687h CCC: $33.50
Publication on Web 11/16/2006

is rather widespread in olefin polymerization by nonmetallocenes. We reasoned that the use of salicyloxazoline ligands **V**[9] might provide more stable catalysts, but found that the complexes [CpM(**V**)X_2] were generally inaccessible (vide infra). We report here that, rather counterintuitively, the bulkier complexes based on pentamethylcyclopentadienyl can be synthesized readily. Under the appropriate conditions, these complexes provide single-site polymerization catalysts. Stability and mechanistic studies are also reported.

Results and Discussion

Synthesis of Proligands and Organometallic Complexes. A range of salicyloxazolines H**L**^{n} (n = 1−4) was synthesized from the corresponding salicylic acids and amino alcohols, as previously described,[9,10] or by similar methods (Scheme 1). Treatment with excess NaH in THF produced the sodium salts Na**L**^{n}·xTHF in quantitative yields. These were isolated by filtration and evaporation or used in situ as ligand transfer reagents.

Subsequent treatment of [Cp*MCl_3] (M = Zr,[11] Hf[12]) with Na**L**^{n}·xTHF produced the complexes [Cp*M**L**^{n}Cl_2] (n = 1−4), in reasonable to good yields. Analogous reactions of the indenyl complexes [(η^5-C_9H_7)MCl_3] (M = Ti, Zr, Hf)[13] and [CpZrCl_3(DME)] failed to produce tractable complexes, despite the fact that the latter is a precursor for the phenoxyimine (PI, vide supra) complexes [CpZr(PI)Cl_2].[8] Treatment of [CpTiCl_3][14] with Na**L**^{1} gave the complex [CpTi**L**^{1}Cl_2] in good yield, although the same reaction with the more bulky Na**L**^{2} was unsuccessful. Finally, for comparison with the above, we attempted to synthesize the hitherto unreported complexes [Cp*M(PI)Cl_2] (M = Zr, Hf) from Cp*MCl_3 by various means, but this was ultimately unsuccessful.

Scheme 1

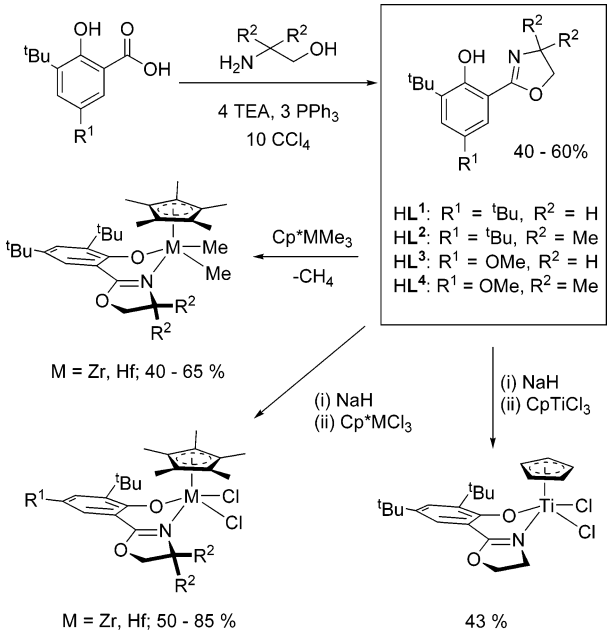

We achieved the syntheses of [Cp*MMe_3] (M = Zr, Hf) by the methods of Bercaw[11] and Marks.[15] Direct reactions thereof with H**L**^{n} (n = 1, 2) produced the four complexes [Cp*ML^n-Me_2] (Scheme 1). The isolated yields were limited by the difficulty in crystallizing these rather soluble complexes; experiments in NMR tubes indicated very high conversions.

Crystallographic Analyses. The molecular structures of several of the complexes have been determined by X-ray crystallography. Table 1 gives crystallographic data, while Table 2 compares key structural parameters for all four structures. Thermal ellipsoid plots are given in Figures 1−3. All of the complexes have a four-legged piano-stool structure. Unsurprisingly, [Cp*Zr**L**^{1}Cl_2] and [Cp*Hf**L**^{1}Cl_2] are isomorphous, having very similar unit cell and other parameters, and suffer from the same lattice solvent disorder (vide infra).

We will compare first the three structures of dichloride complexes (Figures 1 and 2). The M(1)−O(1) distances of ca. 2.02 Å and the C(1)−O(1)−M(1) angles of 137−146° are consistent with sp^2 hybridization at O,[16] and thus the alkoxide acts formally as a three-electron donor. In the structure of [Cp*Zr**L**^{2}Cl_2] steric interactions between the oxazoline methyl group at C(29) and the Cp* ligand cause a fold in the metal chelate ring such that the angle θ between the least-squares planes defined by N(1)−C(7)−C(8)−C(1)−O(1) and N(1)−Zr(1)−O(1) is 21.17(50)°. In the complexes [Cp*M**L**^{1}Cl_2] (M = Zr, Hf), where there is no significant steric pressure in this region, the angles θ are 8.64(18) and 9.23(22)°, respectively. The fold angle ϕ in the oxazoline ring (the angle between the planes defined by N(1)−C(7)−O(2)−C(9) and N(1)−C(8)−C(9)) is also the largest for [Cp*Zr**L**^{2}Cl_2]. As a further consequence, C(1)−O(1)−M(1) for [Cp*Zr**L**^{2}Cl_2] is by far the lowest of the three chloride complexes at 137.1(4)° and the M(1)−N(1) distance is the largest. Interestingly, the M(1)−N(1) distances for the **L**^{1} complexes of 2.295(3) and 2.277(4) Å are rather shorter than those observed for analogous imino-phenolate systems at ca. 2.35 Å,[17] and this may be indicative of a stronger bond resulting from the presence of the conjugated O atom in

(5) (a) Yoon, J.; Mathers, R. T.; Coates, G. W.; Thomas, E. L. *Macromolecules* **2006**, *39*, 1913. (b) Cherian, A. E.; Lobkovsky, E. B.; Coates, G. W. *Macromolecules* **2005**, *38*, 6259. (c) De Rosa, C.; Circelli, T.; Auriemma, F.; Mathers, R. T.; Coates, G. W. *Macromolecules* **2004**, *37*, 9034. (d) Mason, A. F.; Coates, G. W. *J. Am. Chem. Soc.* **2004**, *126*, 10798. (e) Fujita, M.; Coates, G. W. *Macromolecules* **2002**, *35*, 9640. (f) Hustad, P. D.; Coates, G. W. *J. Am. Chem. Soc.* **2002**, *124*, 11578. (g) Hustad, P. D.; Tian, J.; Coates, G. W. *J. Am. Chem. Soc.* **2002**, *124*, 3614. (h) Tian, J.; Coates, G. W. *Angew. Chem., Int. Ed.* **2000**, *39*, 3626.

(6) (a) Gomez, R.; Green, M. L. H.; Haggitt, J. L. *J. Chem. Soc., Chem. Commun.* **1994**, *22*, 2607. (b) Chernega, A. N.; Gomez, R.; Green, M. L. H. *J. Chem. Soc., Chem. Commun.* **1993**, *18*, 1415. (c) Gomez, R.; Duchateau, R.; Chernega, A. N.; Teuben, J. H.; Edelmann, F. T.; Green, M. L. H. *J. Organomet. Chem.* **1995**, *491*, 153. (d) Jayaratne, K. C.; Sita, L. R. *J. Am. Chem. Soc.* **2000**, *122*, 958. (e) Keaton, R. J.; Jayaratne, K. C.; Henningsen, D. A.; Koterwas, L. A.; Sita, L. R. *J. Am. Chem. Soc.* **2001**, *123*, 6197. (f) Kissounko, D. A.; Fettinger, J. C.; Sita, L. R. *Inorg. Chim. Acta* **2003**, *345*, 121. (g) Zhang, Y. H.; Reeder, E. K.; Keaton, R. J.; Sita, L. R. *Organometallics* **2004**, *23*, 3512. (h) Kissounko, D. A.; Zhang, Y. H.; Harney, M. B.; Sita, L. R. *Adv. Synth. Catal.* **2005**, *347*, 426. (i) Zhang, Y. H.; Sita, L. R. *Chem. Commun.* **2003**, *18*, 2358. (j) Koterwas, L. A.; Fettinger, J. C.; Sita, L. R. *Organometallics* **1999**, *18*, 4183. (k) Sita, L. R.; Babcock, J. R. *Organometallics* **1998**, *17*, 5228.

(7) Doherty, S.; Errington, R. J.; Jarvis, A. P.; Collins, S.; Clegg, W.; Elsegood, M. R. J. *Organometallics* **1998**, *17*, 3408.

(8) Bott, R. K. J.; Hughes, D. L.; Schormann, M.; Bochmann, M.; Lancaster, S. J. *J. Organomet. Chem.* **2003**, *665*, 135.

(9) Bott, R. K. J.; Hammond, M. L.; Horton, P. N.; Lancaster, S. J.; Bochmann, M.; Scott, P. *Dalton Trans.* **2005**, *22*, 3611.

(10) (a) Westmoreland, I.; Munslow, I. J.; Clarke, A. J.; Clarkson, G.; Deeth, R. J.; Scott, P. *J. Organomet. Chem.* **2006**, *691*, 2228. (b) Vorbruggen, H.; Krolikiewicz, K. *Tetrahedron* **1993**, *49*, 9353. (c) Vorbruggen, H.; Krolikiewicz, K. *Tetrahedron Lett.* **1981**, *22*, 4471.

(11) Wolczanski, P. T.; Bercaw, J. E. *Organometallics* **1982**, *1*, 793.

(12) Roddick, D. M.; Fryzuk, M. D.; Seidler, P. F.; Hillhouse, G. L.; Bercaw, J. E. *Organometallics* **1985**, *4*, 97.

(13) Morris, R. J.; Shaw, S. L.; Jefferis, J. M.; Storhoff, J. J.; Goedde, D. M. *Inorg. Synth.* **1998**, *32*, 215.

(14) Mach, K.; Varga, V.; Antropiusova, H.; Polacek, J. *J. Organomet. Chem.* **1987**, *333*, 205.

(15) Schock, L. E.; Marks, T. J. *J. Am. Chem. Soc.* **1988**, *110*, 7701.

(16) Bei, X. H.; Swenson, D. C.; Jordan, R. F. *Organometallics* **1997**, *16*, 3282.

Table 1. Crystallographic Data, Collection Parameters, and Refinement Parameters for [Cp*ZrL^{1}Me$_2$], [Cp*HfL^{1}Cl$_2$], [Cp*ZrL^{2}Cl$_2$], and [Cp*ZrL^{1}Cl$_2$]

	[Cp*Zr**L**^{1}Cl$_2$]·0.25Et$_2$O	[Cp*Zr**L**^{1}Me$_2$]	[Cp*Zr**L**^{2}Cl$_2$]	[Cp*Hf**L**^{1}Cl$_2$]·0.25Et$_2$O
empirical formula	$C_{28}H_{41.5}Cl_2NO_{2.25}Zr$	$C_{29}H_{45}NO_2Zr$	$C_{29}H_{43}Cl_2NO_2Zr$	$C_{28}H_{41.5}Cl_2HfNO_{2.25}$
fw	599.76	530.88	599.76	677.51
cryst size (mm^3)	0.18 × 0.15 × 0.14	0.32 × 0.10 × 0.06	0.18 × 0.15 × 0.14	0.25 × 0.23 × 0.08
cryst syst	monoclinic	triclinic	monoclinic	monoclinic
space group	$P2_1/n$	$P\bar{1}$	$P2_1$	$P2_1/n$
a (Å)	9.8486(3)	10.5992(15)	9.4657(6)	9.9224(2)
b (Å)	13.7408(4)	11.5384(17)	16.7741(10)	13.8597(3)
c (Å)	22.8455(6)	12.7577(19)	9.6448(6)	23.0046(5)
α (deg)	90	64.097(3)	90	90
β (deg)	98.4590(10)	82.870(3)	102.54	98.5900(10)
γ (deg)	90	82.570(3)	90	90
V (Å^3)	3057.99(15)	1387.7(4)	1494.86(16)	3128.14(11)
D_{calcd} (Mg/m^3)	1.282	1.271	1.332	1.439
μ (mm^{-1})	0.558	0.420	0.571	3.529
F_{000}	1234	564	628	1362
total no. of rflns	19 166	17 565	9665	19 282
no. of indep rflns	7387	6698	6630	7376
R_{int}	0.0912	0.0506	0.0805	0.0600
no. of data/restraints/ params	7387/2/322	6698/0/311	6630/1/330	7376/4/327
R1 ($I > 2\sigma(I)$)	0.0536	0.0431	0.0669	0.0389
wR2	0.1314	0.0834	0.1398	0.0938
GOF on F^2	0.914	0.962	0.873	0.968

Table 2. Selected Bond Lengths (Å) and Angles (deg) for [Cp*ZrL^{1}Me$_2$], [Cp*HfL^{1}Cl$_2$], [Cp*ZrL^{2}Cl$_2$], and [Cp*ZrL^{1}Cl$_2$]

	[Cp*Zr**L**^{1}Cl$_2$]	[Cp*Hf**L**^{1}Cl$_2$]	[Cp*Zr**L**^{2}Cl$_2$]	[Cp*Zr**L**^{1}Me$_2$]
M(1)−O(1)	2.004(3)	2.021(3)	2.013(5)	2.0275(15)
M(1)−Cl(1)	2.4577(11)	2.4550(12)	2.441(2)	
M(1)−Cl(2)	2.4641(11)	2.4642(12)	2.4758(19)	
Zr(1)−C(30)				2.282(3)
Zr(1)−C(31)				2.270(2)
M(1)−N(1)	2.295(3)	2.277(4)	2.358(5)	2.3598(19)
M(1)−Cp*$_{CEN}$	2.214	2.216	2.217	2.231
Cl(1)−M(1)−Cl(2)	87.66(4)	86.91(4)	85.02(7)	
N(1)−M(1)−Cl(2)	143.21(8)	142.25(11)	144.20(15)	
N(1)−M(1)−Cl(1)	81.77(8)	81.79(10)	86.4(2)	
C(30)−Zr(1)−C(31)				84.23(10)
O(1)−M(1)−N(1)	75.91(10)	76.50(13)	76.00(19)	74.18(6)
C(1)−O(1)−M(1)	145.6(2)	144.1(3)	137.1(4)	147.14(15)
C(7)−N(1)−M(1)	128.0(3)	128.1(3)	122.4(5)	127.77(16)
θ^a	8.64	9.23	21.17	10.52
ϕ^b	14.23	14.45	20.04	13.01

[a] The angle θ is defined as the angle between the planes defined by N(1)−C(7)−C(8)−C(1)−O(1) and N(1)−Zr(1)−O(1). [b] The angle ϕ is defined as the angle between the planes defined by N(1)−C(7)−O(2)−C(9) and N(1)−C(8)−C(9).

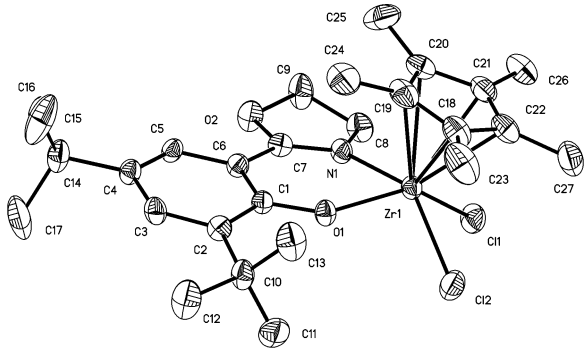

Figure 1. Molecular structure of [Cp*Zr**L**^{1}Cl$_2$]. [Cp*Hf**L**^{1}Cl$_2$] is isomorphous.

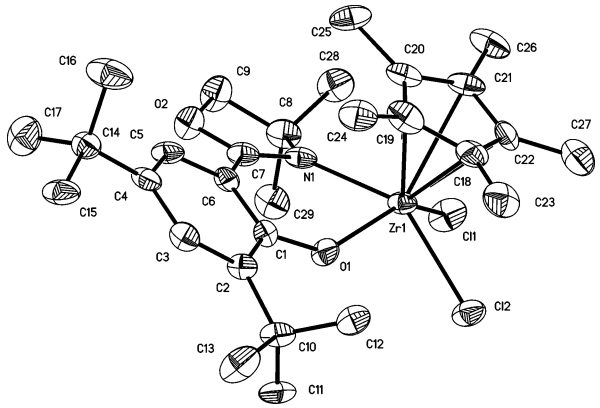

Figure 2. Molecular structure of [Cp*Zr**L**^{2}Cl$_2$].

the oxazoline ring. The steric demand of the proligand has little effect on the Cl(1)−M−Cl(2) angle (all 85−88°), although the N(1)−Zr(1)−Cl(1) angle in [Cp*Zr**L**^{2}Cl$_2$] is ca. 4° larger than in the complexes of **L**^{1}.

In [Cp*Zr**L**^{1}Me$_2$] (Figure 3) the Zr(1)−O(1) and Zr(1)−N(1) distances at 2.0275(15) and 2.3598(19) Å, respectively, are significantly longer than those in the analogous chloride complex [Cp*Zr**L**^{1}Cl$_2$] at 2.004(3) and 2.295(3) Å, as expected on the basis of electrostatics (Cl more electronegative than Me). In other respects the last two structures are very alike, and other structural parameters are similar to those observed in analogous systems.[6g,18]

(17) (a) Knight, P. D.; Clarkson, G.; Hammond, M. L.; Kimberley, B. S.; Scott, P. *J. Organomet. Chem.* **2005**, *690*, 5125. (b) Matsui, S.; Mitani, M.; Saito, J.; Tohi, Y.; Makio, H.; Matsukawa, N.; Takagi, Y.; Tsuru, K.; Nitabaru, M.; Nakano, T.; Tanaka, H.; Kashiwa, N.; Fujita, T. *J. Am. Chem. Soc.* **2001**, *123*, 6847.

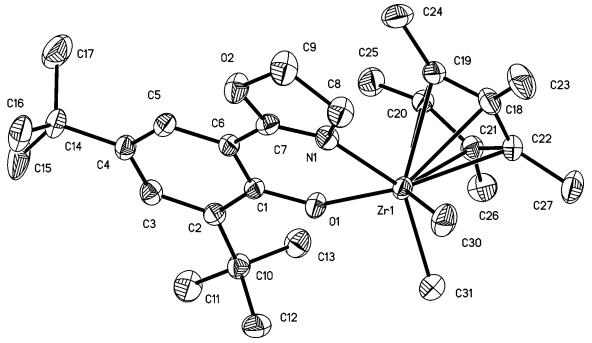

Figure 3. Molecular structure of [Cp*Zr**L**^{1}Me$_2$].

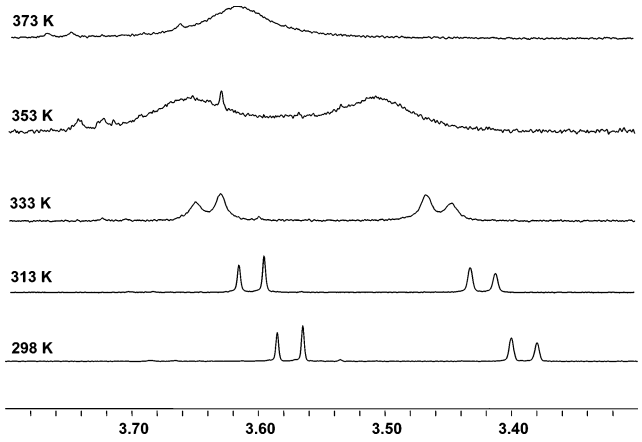

Figure 4. Variable-temperature ^{1}H NMR spectra of [Cp*Zr**L**^{2}Me$_2$].

VT NMR Studies. The chirality of all the complexes described above is manifest in their ^{1}H NMR spectra at ambient temperature. For example, in [Cp*Zr**L**^{1}Cl$_2$] all four oxazoline protons are inequivalent, giving rise to mutually coupled complex multiplets around 3.50 and 3.77 ppm (1H each), and two overlapping multiplets between 3.36 and 3.46 ppm (2H total). In [Cp*Zr**L**^{2}Cl$_2$] a pair of doublets is observed at ca. 3.35 and 3.49 ppm and the two oxazoline methyl groups appear as separate singlets at 1.04 and 1.49 ppm. In [Cp*Zr**L**^{1}Me$_2$] the oxazoline CH_2 groups appear as four distinct multiplets, and the zirconium-bound methyl groups are also inequivalent (0.03 and 0.41 ppm, and 37.5 and 39.4 ppm in the ^{13}C NMR spectrum).

We recorded the temperature dependence of the ^{1}H NMR spectra for [Cp*Zr**L**^{1}Me$_2$] and [Cp*Zr**L**^{2}Me$_2$]. Figure 4 shows the oxazoline H atom region for [Cp*Zr**L**^{2}Me$_2$]. At 298 K, these are observed as two mutually coupled AB doublets. As the temperature is increased, the peaks broaden and then coalesce at ca. 373 K. These spectra are consistent with exchange between enantiomers (racemization).[19] A line shape analysis[20] gave exchange rate data for this process (Figure 5). The thermodynamic parameters thus extracted are shown in Table 3 along with the values for $\Delta G^{\ddagger}_{298}$ calculated directly using eq 1.[21]

$$\Delta G^{\ddagger} = aT[10.319 + \log(T/k)] \qquad a = 0.01914 \qquad (1)$$

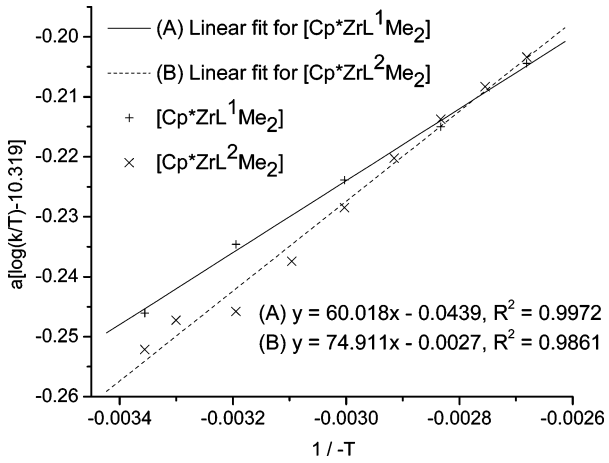

Figure 5. Eyring plot for [Cp*Zr**L**^{2}Me$_2$].

Table 3. Data from Eyring Plots[a] for $\Delta G^{\ddagger}$, $\Delta H^{\ddagger}$, and $\Delta S^{\ddagger}$

complex	$\Delta H^{\ddagger}$/ kJ mol^{-1}	$\Delta S^{\ddagger}$/ J K^{-1} mol^{-1}	$\Delta G^{\ddagger}_{298}$/ kJ mol^{-1}	$\Delta G^{\ddagger}_{298}$[b]/ kJ mol^{-1}
[Cp*Zr**L**^{1}Me$_2$]	60.0 ± 1.9	−43.9 ± 5.6	73.1 ± 3.5	73.3 ± 1.5
[Cp*Zr**L**^{2}Me$_2$]	74.9 ± 3.4	−2.0 ± 10	75.7 ± 6.2	75.1 ± 1.1

[a] Data were obtained from line-shape analysis unless otherwise noted. [b] Data were obtained from eq 1.

For each individual complex the two methods lead to the same value for $\Delta G^{\ddagger}$ within standard errors.[22,23] Notably, the values of $\Delta G^{\ddagger}$ for the two complexes are effectively the same, but the entropy of activation component is much more negative for the complex of **L**^{1} than for that of **L**^{2}. This may be related to the rather more "ordered" structure of the complex [Cp*Zr**L**^{2}Me$_2$] compared to that of [Cp*Zr**L**^{1}Me$_2$]; in the latter the salicyloxazoline ligand is free to hinge about the N−O vector, whereas in the former it is rather fixed in position. In any event, the similarity of $\Delta G^{\ddagger}$ values between the two complexes is consistent with an N-dissociative mechanism for racemization; a rotation-in-place mechanism would give a comparatively high value for [Cp*Zr**L**^{2}Me$_2$], as a result of steric interactions between methyl groups on the oxazoline ring and the Cp* ligand. We cannot, however, exclude the possibility that the two complexes undergo exchange by different mechanisms; on the basis that the more sterically encumbered system [Cp*Zr**L**^{2}Me$_2$] would be the most likely of the two to undergo N-dissociative exchange, we would expect this compound to have the most positive $\Delta S^{\ddagger}$ value, which is indeed the case.

Ethylene Polymerization Studies. The complexes [Cp*M**L**^{n}X$_2$] (M = Zr, Hf; n = 1, 2; X = Cl, Me) and [CpTi**L**^{1}Cl$_2$] were tested for activity in ethylene polymerization (Table 4). The zirconium complexes exhibited a range of productivities, varying with the nature of the salicyloxazoline coligand, conditions, and cocatalyst, whereas the hafnium complexes showed essentially no activity regardless of experimental conditions.

Treatment of [Cp*Zr**L**^{n}X$_2$] with 1000 equiv of MAO cocatalyst at 1.2 bar of ethylene pressure (runs 1−4) gave the most

(18) Zhang, Y. H.; Kissounko, D. A.; Fettinger, J. C.; Sita, L. R. *Organometallics* **2003**, *22*, 21.

(19) Although we have not formally excluded the possibility of a mechanism involving Zr−O bond cleavage, this is very unlikely under these conditions.

(20) Line shape analysis was carried out using WIN-DYNA 32, version 1.01, release 981101, Bruker Analytik GmbH, 1994−1998.

(21) Sandström, J. In *Dynamic NMR Spectroscopy*; Academic Press: London, 1982; pp 93−123.

(22) Hamilton, L. C. In *Regression With Graphics-A Second Course in Applied Statistics*; Brooks/Cole: Belmont, CA, 1991; pp 29−64. Blank, L. In *Statistical Procedures for Engineering, Management and Science*; McGraw-Hill: New York, 1980; pp 487−515.

(23) The standard errors involved in the Eyring plot were calculated using Origin 7.0. The error involved in the single equation is based upon an error in T of ±1 K and an error in k of ±40%. This error value for k comes from the largest deviation from the linear fit in the Eyring plot.

Table 4. Polymerization of Ethene and Hexene Using [Cp*ZrL^{n}X$_2$]

run no.	precat.	amt of cat./ μmol	cocat.	amt of cocat/ equiv	cocat concn/M	Al concn/ M	temp/ °C	av productivity/ 1g (mol bar h)$^{-1}$	M_n	M_w
1[a]	[Cp*ZrL^{1}Cl$_2$]	2.1	MAO	1000		1.2×10^{-2}	30	1.5×10^5	2 340	460 000
2[a]	[Cp*ZrL^{1}Me$_2$]	11	MAO	1000		6.5×10^{-2}	30	8.5×10^4	1 640	266 000
3[a]	[Cp*ZrL^{2}Cl$_2$]	12	MAO	1000		7.1×10^{-2}	30	8.8×10^4	5 750	126 000
4[a]	[Cp*ZrL^{2}Me$_2$]	18	MAO	1000		0.10	30	3.4×10^3		
5[a]	[CpTiL^{1}Cl$_2$]	9.8	MAO	1000		5.6×10^{-2}	30	1.7×10^3		
6[a]	[Cp*ZrL^{1}Cl$_2$]	11	**1**	1.1	7.48×10^{-5}	3.74×10^{-3}	30	2.3×10^5	32 200	644 000
7[a]	[Cp*ZrL^{1}Cl$_2$]	11	**2**	1.1	5.3×10^{-5}	2.43×10^{-3}	30	1.9×10^5	28 600	59 600
8[b]	[Cp*ZrL^{1}Cl$_2$]	11	**1**	1.1	7.48×10^{-5}	3.74×10^{-3}	30	5.6×10^4	18 900	47 000
9[b]	[Cp*ZrL^{1}Cl$_2$]	11	**2**	1.1	5.3×10^{-5}	2.43×10^{-3}	30	8.7×10^4	4 660	445 000
10[c]	[Cp*ZrL^{1}Cl$_2$]	11	**2**	1.1	1.1×10^{-4}	6.05×10^{-3}	30	2.7×10^5	12 000	39 300
11[c]	[Cp*ZrL^{1}Cl$_2$]	1.8	**2**	6.6	1.1×10^{-4}	6.05×10^{-3}	70	1.0×10^6	4 680	24 000
12[c]	[Cp*ZrL^{2}Cl$_2$]	10	**2**	1.1	1.1×10^{-4}	6.05×10^{-3}	30	5.3×10^4	8 660	63 000
13[c]	[Cp*ZrL^{2}Cl$_2$]	10	**2**	1.1	1.1×10^{-4}	6.05×10^{-3}	70	9.0×10^4	5 560	37 300
14[c]	[Cp*ZrL^{3}Cl$_2$]	13	**2**	1.1	1.1×10^{-4}	6.05×10^{-3}	30	7.0×10^4	14 400	44 000
15[c]	[Cp*ZrL^{3}Cl$_2$]	1.8	**2**	6.6	1.1×10^{-4}	6.05×10^{-3}	70	6.1×10^5	4 650	67 900
16[c]	[Cp*ZrL^{4}Cl$_2$]	11	**2**	1.1	1.1×10^{-4}	6.05×10^{-3}	30	2.7×10^4	13 100	51 100
17[c]	[Cp*ZrL^{4}Cl$_2$]	11	**2**	1.1	1.1×10^{-4}	6.05×10^{-3}	70	1.3×10^5	12 500	109 000
18[d]	[Cp*ZrL^{1}Cl$_2$]	11	**2**	1.1	1.1×10^{-4}	6.05×10^{-3}	30	8.5×10^4 (5.2)[e]	18 800	49 900
19[d]	[Cp*ZrL^{2}Cl$_2$]	10	**2**	1.1	1.1×10^{-4}	6.05×10^{-3}	30	3.3×10^4 (trace)[e]	5 650	28 700
20[d]	[Cp*ZrL^{3}Cl$_2$]	13	**2**	1.1	1.1×10^{-4}	6.05×10^{-3}	30	1.4×10^5(2.7)[e]	22 800	52 800
21[d]	[Cp*ZrL^{4}Cl$_2$]	11	**2**	1.1	1.1×10^{-4}	6.05×10^{-3}	30	2.7×10^4 (0.4)[e]	10 500	41 800

[a] Solvent toluene (180 mL). [b] Solvent bromobenzene (100 mL). [c] Solvent toluene (100 mL). [d] Solvent 20 wt % 1-hexene in toluene (100 mL). [e] 1-Hexene contents (mol %) in parentheses.

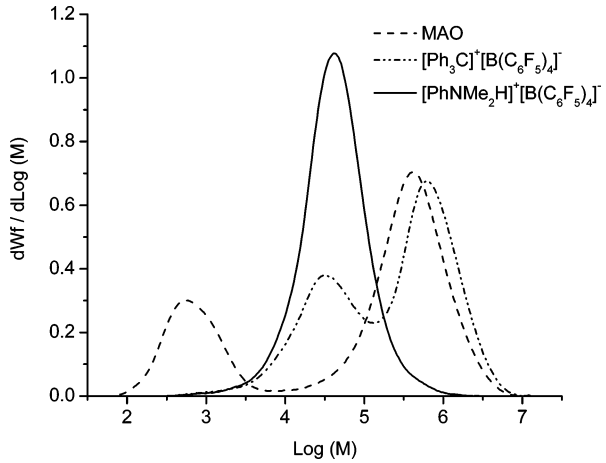

Figure 6. GPC data for PE from [Cp*ZrL^{1}Cl$_2$] and various activators.

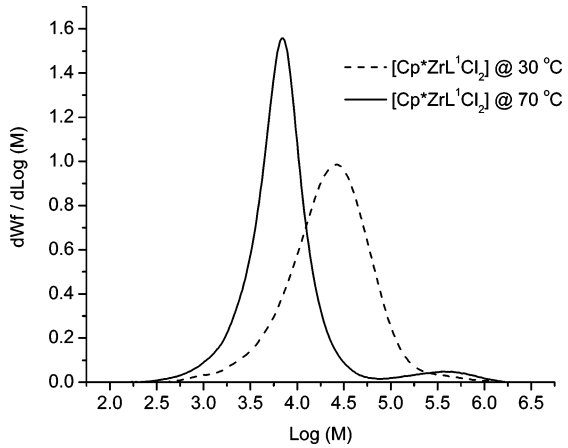

Figure 7. GPC data for PE from [Cp*ZrL^{1}Cl$_2$].

promising results for [Cp*ZrL^{1}Cl$_2$], the bulkier ligand L^2 giving consistently lower productivity. Surprisingly, the complexes X = Me led to relatively poor catalysts. Also, [CpTiL^{1}Cl$_2$] (run 5) has low productivity; the analogous imino-phenolate complexes gave ca. 1.0×10^4−2.0×10^5 g of PE (mol bar h)$^{-1}$ under very similar conditions.[8]

The stoichiometric activators [Ph$_3$C][B(C$_6$F$_5$)$_4$] (**1**) and [PhNMe$_2$H][B(C$_6$F$_5$)$_4$] (**2**), when used in conjunction with AlBu$^i_3$ as an alkylating agent and scavenger, were significantly more productive (runs 6 and 7). The variation of cocatalyst also leads to interesting changes in the physical properties of the polymers produced (Figure 6). Polyethylene produced when either MAO or **1**/AlBu$^i_3$ is used as the cocatalyst has a bimodal molecular weight distribution, consistent with the formation of more than one active species (vide infra). The use of **2** gives a unimodal distribution with a narrow PDi (2.1), characteristic of single-site catalysis. In contrast, precatalysts [CpM(PI)Cl$_2$] gave multimodal molecular weight distributions, although only activation with MAO was reported.[8]

Sita has shown that chlorobenzene is a more successful solvent than toluene for the polymerization and copolymerization of alkenes with related half-sandwich group 4 catalysts.[24] We found that for [Cp*ZrL^{1}Cl$_2$] activated with **1** or **2** the opposite is the case (runs 8 and 9). The molecular weights of the polymers produced in chlorobenzene are also slightly lower than those in toluene.

We have been concerned with the thermal stability and deactivation mechanisms of PI and related catalyst systems[9,17a] and thus tested the most active of the current catalysts using a gas delivery measurement system in order to profile the catalyst activity over time, at a constant temperature. The average productivities for these runs (runs 10−17) calculated from the isolated yield of polyethylene in a 1 h run correlated well with the measured gas flow and with earlier runs.[25] The average productivity of each catalyst is higher at 70 °C than at 30 °C, particularly in the case of [Cp*ZrL^{1}Cl$_2$], which at 1.0×10^6 g of PE (mol bar h)$^{-1}$ is highly active.[3b] Molecular weight distributions from GPC of the polymers thus made at 30 °C (run 10) and 70 °C (run 11) are shown in Figure 7. At the lower temperature, the polymer (unimodal, PDI = 3.3) is similar to that from run 7. At 70 °C there is a reduction in molecular

(24) (a) Jayaratne, K. C.; Keaton, R. J.; Henningsen, D. A.; Sita, L. R. *J. Am. Chem. Soc.* **2000**, *122*, 10490. (b) Jayaratne, K. C.; Sita, L. R. *J. Am. Chem. Soc.* **2000**, *122*, 958.

(25) In the context of catalyst stability studies, a comparison with [Cp*Zr(PI)Cl$_2$] would be instructive, but unfortunately we have thus far been unable to synthesise these compounds (vide supra).

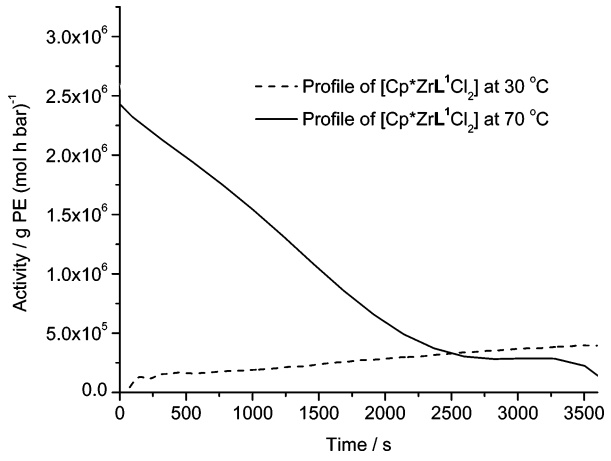

Figure 8. Ethylene polymerization activity profile of [Cp*Zr**L**^{1}Cl$_2$].

weight of the main peak and a small amount of higher molecular weight polymer was also formed, presumably as a result of catalyst decomposition to another active species at this higher temperature.

The activity profiles of [Cp*Zr**L**^{1}Cl-$_2$] at 30 and 70 °C (runs 10 and 11) are shown in Figure 8. After an initial induction period the activity of [Cp*Zr**L**^{1}Cl$_2$] increases steadily across a 1 h run at 30 °C. This may be due to a relatively low rate of activation of the precatalyst with $AlBu^i_3$ and [$PhNMe_2H$]-[$B(C_6F_5)_4$] (vide infra); unfortunately, preactivation of the catalyst for longer periods generally led to poor activity on admission of ethylene gas. At 70 °C uptake of ethylene is observed instantaneously and the initial rate of polymerization is ca. 2.4×10^6 g of PE (mol bar h)$^{-1.}$ This decreases fairly steadily over 1 h, with $t_{1/2} = 20$ min, although after 1 h the activity is still a moderate, 2.8×10^5 g of PE (mol bar h)$^{-1}$. Under the same conditions, [Cp*Zr**L**^{2}Cl$_2$] showed an initial activity an order of magnitude lower at 2.9×10^5 g of PE (mol bar h)$^{-1}$ and decomposed much more rapidly ($t_{1/2}$ ca. 5 min). [Cp*Zr**L**^{2}Cl$_2$] also decomposed at 30 °C, with $t_{1/2} = 11$ min (runs 12 and 13). Since the mechanism of catalyst death is most probably transfer of the salicyloxazoline ligand to aluminum (vide infra), the relative instability of the catalyst derived from [Cp*Zr**L**^{2}Cl$_2$] may be an effect of the larger angle θ for the **L**^{2} complex (Table 2), leading to greater accessibility of the phenolate oxygen atom to attack by Al^iBu_3.

Fujita noted that the introduction of a methoxy group para to the phenolate O atom in certain [$Zr(PI)_2Cl_2$] complexes led to higher productivities.[26] While it is not apparent whether this arises from an improvement in intrinsic activity or reduction in the rate of catalyst decomposition, we decided to investigate the effect on the present salicyloxazoline system (ligands **L**^{3} and **L**^{4}). In runs 14 and 15, [Cp*Zr**L**^{3}Cl$_2$] showed a slightly lower average productivity than [Cp*Zr**L**^{1}Cl$_2$] but at 70 °C was rather longer lived; with $t_{1/2} = 27.5$ min [Cp*Zr**L**^{4}Cl$_2$] (runs 16 and 17) behaved similarly ($t_{1/2} = 30$ min) at this higher temperature. The thermal stability of the catalyst does thus appear to improve with the introduction of a *p*-methoxy group, without substantially altering the productivity.

Ethylene/1-Hexene Copolymerizations. While propene and hexene were not homopolymerized to a significant degree by the present catalysts, ethylene/hexene copolymers were produced (runs 18−21). The hexene content of the polymer was determined by ^{13}C NMR spectroscopy using the method of Hsieh and Randall.[27] The catalysts incorporating the bulkier salicyloxazolines, i.e., [Cp*Zr**L**^{2}Cl$_2$] and [Cp*Zr**L**^{4}Cl$_2$], gave very low or negligible incorporation compared with [Cp*Zr**L**^{1}Cl$_2$] or [Cp*Zr**L**^{3}Cl$_2$]. The rate of ethylene uptake and productivity with [Cp*Zr**L**^{3}Cl$_2$] is higher than with [Cp*Zr**L**^{1}Cl$_2$].

NMR Studies of the Catalyst Activation Process. We studied the reactions of [Cp*Zr**L**^{1}Me$_2$] in d_5-bromobenzene with the cocatalysts used in the above polymerization processes. Treatment with ca. 20 equiv of dried MAO led to broad features in the ^{1}H NMR spectrum, and identification of a product or products was not feasible. In particular the very broad resonance for MAO around 0 ppm obscures the region where metal-bound methyl signals are expected. The reaction with a slight excess of trityl (**1**) and anilinium (**2**) led to complete consumption[28] of the starting materials and production of a major new organometallic species, common to both experiments. The ^{1}H NMR spectrum is consistent with the formulation [Cp*Zr**L**^{1}Me]-[$B(C_6F_5)_4$] (Figure 9). The oxazoline region reveals that, like the starting material, this compound is chiral (four mutually coupled oxazoline H atoms), but as can be seen most clearly in Figure 9a, it has only one methyl group (δ 0.24 ppm). The expected coproducts Ph_3CMe and $PhNMe_2$ were also formed in appropriate quantities. A small peak at the correct chemical shift for methane in this solvent (0.142 ppm) was also detected in the reaction with **2**.

The product from **1** (Figure 9b) has a significant impurity of unidentified oxazoline (or similar) species which display resonances in the metal alkyl region (0.02−0.12 ppm) and thus represent potentially catalytic impurities. We speculate that the acid-sensitive oxazoline unit may have taken part in side reactions with the trityl ion. The product from **2** (Figure 9a) included a small amount of a different oxazoline-containing impurity, but there was no corresponding Zr−Me resonance. Our proposal that this arises from the dicationic species [Cp*Zr**L**^{1}(NMe_2Ph)]$^{2+}$ is encouraged by the observation of two distinct resonances at 2.61 and 2.45 ppm (1:1 ratio) with an appropriate integral for the diastereotopic NMe_2 group. Notably, the major species [Cp*Zr**L**^{1}Me][$B(C_6F_5)_4$] does not form an adduct with $PhNMe_2$, even at this relatively high concentration.[29]

The properties of the polymers produced under catalytic conditions by [Cp*Zr**L**^{1}X$_2$] systems are consistent with the information available from the above catalyst activation studies. (i) The [Cp*Zr**L**^{1}Me$_2$]/**2** system gives a single catalytic species (Figure 9b) and a unimodal polymer (Figure 6). (ii) [Cp*Zr**L**^{1}Me$_2$]/**1** gives the same catalyst as **2** along with at least one other potential catalyst; this is also reflected in the GPC data. In addition, we might also speculate that the catalyst species responsible for the higher weight fractions present in the [Cp*Zr**L**^{1}Me$_2$]/**1** and [Cp*Zr**L**^{1}Me$_2$]/MAO polymers arises from reactions of these strong Lewis acids with the oxazoline ligand.

Computational Investigations of the Catalytic Reaction. DFT calculations of the mechanism of the insertion of one ethylene unit into the metal-bound methyl group of [Cp*Zr**L**^{1}Me]$^+$ were carried out.[30] Two general directions of

(26) Matsukawa, N.; Matsui, S.; Mitani, M.; Saito, J.; Tsuru, K.; Kashiwa, N.; Fujita, T. *J. Mol. Catal. A: Chem.* **2001**, *169*, 99.

(27) Hsieh, E. T.; Randall, J. C. *Macromolecules* **1982**, *15*, 1402.

(28) In the case of **2** the reaction took place overnight, although the product alkyl cation was remarkably stable, existing at ambient temperatures for several days in solution before noticeable decomposition.

(29) Bochmann, M.; Lancaster, S. J. *J. Organomet. Chem.* **1992**, *434*, C1.

(30) These studies were carried out without consideration of counteranion and solvent effects.

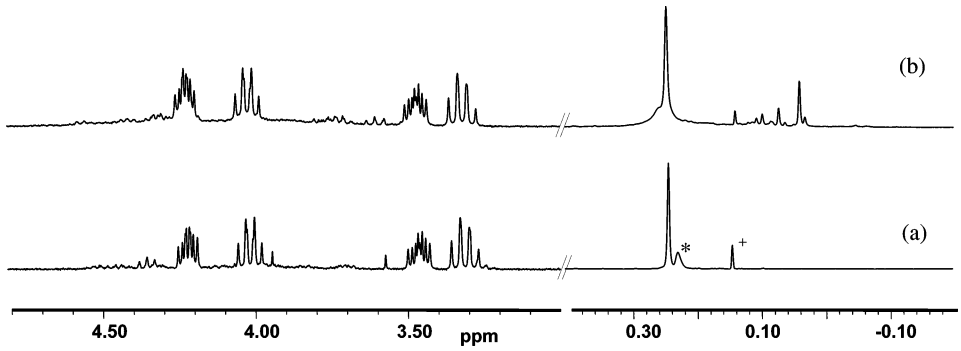

Figure 9. ^{1}H NMR spectra of the reactions of [Cp*Zr**L**^{1}Me$_2$] with (a) [PhNHMe$_2$][B(C$_6$F$_5$)$_4$] and (b) [Ph$_3$C][B(C$_6$F$_5$)$_4$]. The asterisk indicates an impurity of silicone vacuum grease, and the plus sign indicates methane.

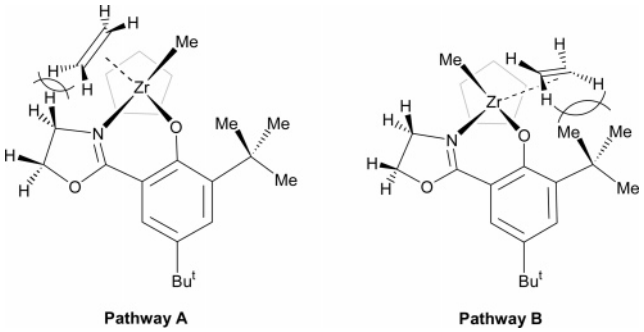

Figure 10. Projections of the computed isomeric structures of [Cp*Zr**L**^{1}Me(C$_2$H$_4$)]$^+$ corresponding to pathways A and B, viewed along the Zr−Cp* centroids.

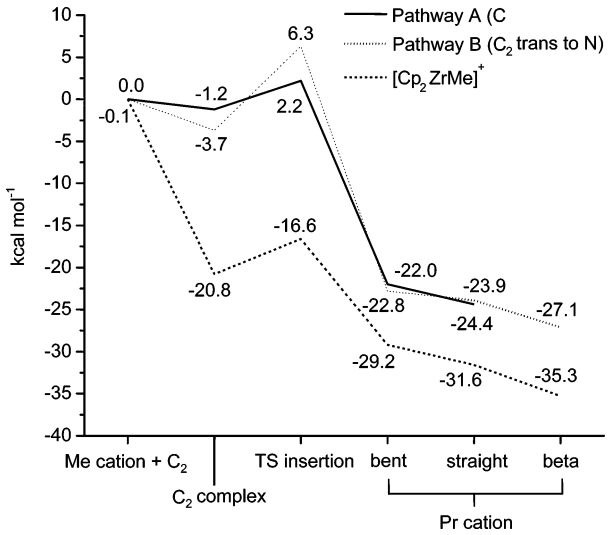

Figure 11. Optimized energy levels, relative to starting materials for the insertion of C_2H_4 into the Zr−Me bond of [Cp$_2$ZrMe]$^+$ and [Cp*Zr**L**^{1}Me]$^+$ along pathways A and B.

approach of the ethylene monomer toward the metal center were considered (Figure 10). The computed energies and selected bond distances are presented in Figure 11 and Table 5, together with the values obtained for [Cp$_2$ZrMe]$^+$ for comparison, calculated at the same level of theory.

The crystallographic paramaters of Cp*Zr**L**^{1}Me$_2$ were used as a starting point for the calculations. Removing one methyl ligand leads to two unoptimized [Cp*Zr**L**^{1}Me]$^+$ complexes with a vacant coordination site trans to either the O or N donor of **L**^{1}. A subsequent geometry optimization leads in both cases to a three-legged piano-stool configuration with nearly equivalent geometry energy (within 0.1 kcal mol^{-1}). Addition of ethylene leads to an intermediate ethylene adduct at 1.2 kcal mol^{-1} (pathway A) and 3.7 kcal mol^{-1} (pathway B) lower in energy than the corresponding Me cation plus free ethylene. A subsequent transition state for insertion of ethylene into the Zr−Me bond was found 3.4 and 10.0 kcal higher in energy, respectively. These barriers are within the range typically calculated for metallocenes and other highly active single-site catalysts.[31] Both transition states have an α-agostic interaction, with the C_γ−H bond of the Zr-bound methyl group lengthened from 1.09 to 1.11 Å and a Zr−H distance of 2.36 Å. The Zr−propyl reaction products are similar in energy for both pathways and are 22.0 and 22.8 kcal mol^{-1} below the sum of energies of the reactants. In neither structure was a γ-agostic interaction observed. The complex adopts a distorted three-legged piano-stool configuration with the propyl chain bent toward the former ethylene coordination site. Chain straightening leads in both cases to a nearly symmetrical piano-stool configuration, with the perfectly staggered propyl chain directed away from the Cp* ring and an additional energy release of 2.4 kcal mol^{-1} (pathway A) and 1.1 kcal mol^{-1} (pathway B). A β-agostic confomer was only found for pathway B, with the agostic interaction trans to the oxygen donor and an additional energy release of 3.2 kcal mol^{-1}. In this structure the C_β−H bond of the agostic hydrogen is lengthened to 1.15 Å and the Zr−H distance is 2.22 Å. No attempts were made to determine the barriers for these propyl chain isomerizations.

For [Cp$_2$ZrPr]$^+$, all confomers contain agostic ineractions. In addition to the strong β-agostic ineraction with one β-H in the "beta" isomer, two weaker interactions with both β-H in the "straight" isomer and an interaction with one γ-H in the "bent" isomer can be observed. Structure files for all calculated species are available as Supporting Information.

For [Cp*Zr**L**^{1}Me]$^+$ the ethylene coordination energy (1.2 or 3.7 kcal mol^{-1}) is very low compared to the values for [Cp$_2$ZrMe]$^+$ obtained in this work (20.8 kcal mol^{-1}) and by Ziegler and co-workers.[32] Steric hindrance encountered in the ethylene adduct [Cp*Zr**L**^{1}Me(C$_2$H$_4$)]$^+$, either with the hydrogen atoms in the 4-position on the oxazoline (pathway A) or the *o*-^{t}Bu substituent on the salicyl ring (pathway B) is depicted in Figure 10. The steric constraints imposed by the ligand framework are also evidenced by the absence of any γ-agostic interaction in the [Cp*Zr**L**^{1}Pr]$^+$ insertion products. It is also notable also in this context that in the three-legged piano-stool species [Cp*Zr**L**^{1}Me]$^+$ the methyl group has to move aside in order to accommodate the incoming ethylene ligand. Our optimized structure of [Cp$_2$ZrMe]$^+$, very similar to that produced by Ziegler,[32] is pyramidal and is thus preorganized for coordination of alkene.

(31) Rappé, A. K.; Skiff, W. M.; Casewitt, C. J. *Chem. Rev.* **2000**, *100*, 1435.
(32) Woo, T. K.; Fan, L.; Ziegler, T. *Organometallics* **1994**, *13*, 2252.

Table 5. Calculated Relative Energies (kcal mol^{-1}) and Selected Bond Distances (Å) for Optimized Geometries for the Ethylene Insertion into [Cp*ZrL^{1}Me]$^+$ and [Cp$_2$ZrMe]$^+$

			bond dist							
compd	path	rel energy	Zr−C$_\alpha$	Zr−C$_\beta$	Zr−C$_\gamma$	C$_\alpha$−C$_\beta$	C$_\beta$−C$_\beta$	C$_\alpha$−H^a	C$_\beta$−H^a	C$_\gamma$−H^a
[Cp*ZrL^{1}Me]$^+$ + C$_2$H$_4$	A	0.0			2.24					
[Cp*ZrL^{1}Me(C2H4)]$^+$	A	−1.2	2.26	2.34	2.29	1.40				
TS for C$_2$H$_4$ insertion	A	2.2	2.42	2.72	2.38	1.40	2.22	1.11		
[Cp*ZrL^{1}Me(Pr)]$^+$ (bent)	A	−22.0	2.23			1.53	1.53			
[Cp*ZrL^{1}Me(Pr)]$^+$ (straight)	A	−24.4	2.25			1.54	1.54			
[Cp*ZrL^{1}Me(Pr)]$^+$ (beta)	A					not obsd				
[Cp*ZrL^{1}Me]$^+$ + C$_2$H$_4$	B	−0.1			2.23					
[Cp*ZrL^{1}Me(C$_2$H$_4$)]$^+$	B	−3.7	2.29	2.95	2.97	1.37				
TS for C$_2$H$_4$ insertion	B	6.3	2.44	2.34	2.67	1.41	213	1.11		
[Cp*ZrL^{1}Me(Pr)]$^+$ (bent)	B	−22.8	2.24			1.53	1.53			
[Cp*ZrL^{1}Me(Pr)]$^+$ (straight)	B	−23.9	2.24			1.54	1.54			
[Cp*ZrL^{1}Me(Pr)]$^+$ (beta)	B	−27.1	2.25			1.51		1.15		
[Cp$_2$ZrMe]$^+$ + C$_2$H$_4$		0.0			2.26					
[Cp$_2$ZrMe(C$_2$H$_4$)]$^+$		−20.8	2.84	2.82	2.27					
TS for C$_2$H$_4$ insertion		−16.6	2.41		2.32	1.41	2.19	1.14		
[Cp$_2$ZrMe(Pr)]$^+$ (bent)		−29.2	2.24			1.56	1.57			1.12
[Cp$_2$ZrMe(Pr)]$^+$ (straight)		−31.6	2.26			1.53	1.55		1.11	
[Cp$_2$ZrMe(Pr)]$^+$ (beta)		−35.3	2.28			1.50	1.53		1.17	

^{a} C−H bond distances for agostic hydrogens.

The optimized structures for the [Cp*ZrL^{1}Me(C$_2$H$_4$)]$^+$ intermediates in both pathways show a considerable difference in their Zr−ethylene bond distances: 2.26 and 2.34 Å (pathway A) versus 2.95 and 2.97 Å (pathway B). A cut through the total electron density map along the O−Zr−N plane for both intermediates (Figure 12) reveals a weaker electron density along the Zr−N bond compared to that along the Zr−O bond. This weaker electron-donating capability of the nitrogen donor should render the coordination site trans to N more electrophilic and hence strengthen the Zr−ethylene bond. However, the Zr−C bond distances at this site are longer than those in the trans-O site. This implies that the ethylene addition at the site trans to nitrogen is disfavored for purely steric reasons. This is in agreement with the absence of a β-agostic interaction at the trans-N site.

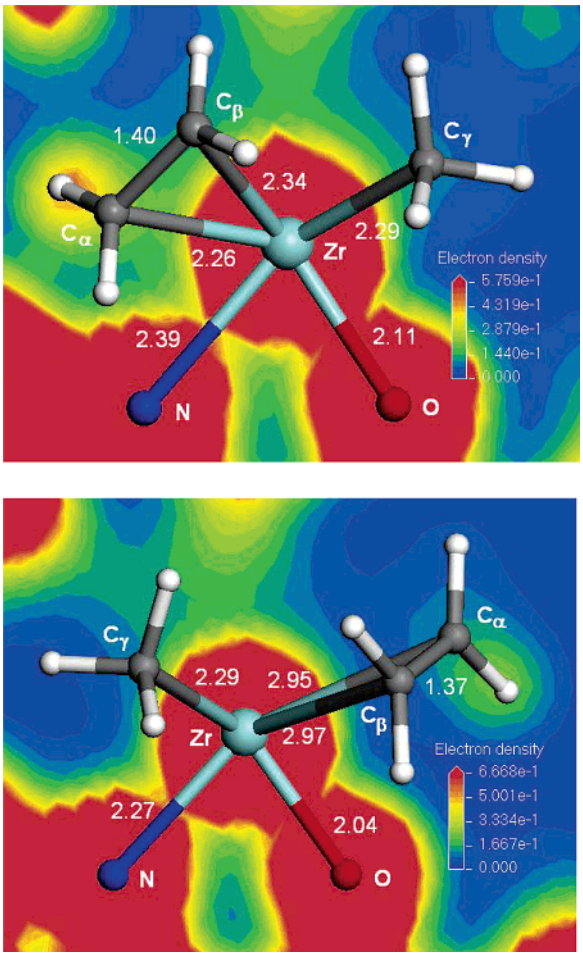

Figure 12. Total electron density in the N−Zr−O plane for [Cp*ZrL^{1}Me(C$_2$H$_4$)]$^+$ from pathways A (upper) and B (lower). Cp* and the remaining salicyloxazoline ligand are removed for clarity.

Conclusions

A new series of group 4 half-sandwich salicyloxazoline complexes bearing Cp* ligands has provided new precatalysts for alkene polymerization. Of the catalyst activators studied, [PhNMe$_2$H][B(C$_6$F$_5$)$_4$] is the best matched, smoothly producing the single, chiral, catalytically competent species [Cp*ZrL^{1}Me][B(C$_6$F$_5$)$_4$] and subsequently promoting the highly active single-site polymerization of ethene (and less active copolymerization of ethene/hexene). The Lewis acidic activator [Ph$_3$C][B(C$_6$F$_5$)$_4$] produces the same catalyst and at least one other, perhaps through a reaction of the basic oxazoline unit. Activation with MAO leads to a qualitatively different and less well-defined system.

This type of catalyst is sensitive to steric effects, and light is cast on the origins of this by the structural and computational work. Approach of ethene to either coordination site is hampered by the *o*-^{t}Bu substituents on the salicyl ring or the oxazoline 4-substituents (R^2), even in the least sterically demanding cases (**L^1** and **L^3**, where R^2 = H). This reluctance to coordinate ethylene is at the heart of the modest (by metallocene standards) productivity of these catalysts in ethylene polymerization. The stability of the three-legged piano-stool structure [Cp*ZrL^{1}Me]$^+$ (observed in the NMR experiments; e.g., Figure 9) is also reflected in the fact that it does not coordinate dimethylaniline. The catalysts based on **L^2** and **L^4** (R^2 = Me) have intrinsic activities at least an order of magnitude lower. They also decompose more rapidly, probably because a structural change caused by the greater steric demand makes the phenoxide unit susceptible to ligand transfer to aluminum in the cocatalyst mixture.

Interestingly, the introduction of a *p*-methoxy substituent has a more profound effect on stability than it does on activity,

commensurate with the growing body of evidence for a mechanism of catalyst death in phenoxyimine and related systems by ligand loss.[9,33]

Experimental Details

General Comments. Air-sensitive procedures were carried out under an inert atmosphere of argon using a dual-manifold vacuum/argon line and standard Schlenk techniques or in an MBraun dry box (<5 ppm of O_2/H_2O). Solvents were dried by refluxing for 3 days under dinitrogen over the appropriate drying agents (sodium for toluene; potassium for THF; sodium−potassium alloy for diethyl ether and pentane; calcium hydride for dichloromethane, acetonitrile, and 1-hexene) and were degassed before use. Solvents were stored in glass ampules under argon. All glassware and cannulas were stored in an oven >373 K. Deuterated solvents were freeze−thaw degassed and dried by refluxing over potassium (for benzene, toluene, and THF) or calcium hydride (for dichloromethane, pyridine, and bromobenzene) for 3 days before trap-to-trap distillation and storage in the drybox. Deuterated chloroform was dried in the bottle over molecular sieves (4 Å).

Cp*$ZrCl_3$,[11] Cp*$HfCl_3$,[11] Cp*$ZrMe_3$,[11] Cp*$HfMe_3$,[15] and $CpTiCl_3$[14] were synthesized using literature methods. Unless stated otherwise, purchased chemical reagents were used as received. Triethylamine and carbon tetrachloride were dried by refluxing under dinitrogen over calcium hydride for 3 days. Triphenylphosphine was recrystallized from hot hexanes and dried under vacuum. A sodium hydride dispersion in mineral oil was placed in a Schlenk vessel under an inert atmosphere and washed three times with diethyl ether to remove the oil. The solid was subsequently dried thoroughly and stored in the glovebox. Flash chromatography was performed with a FlashMaster Personal chromatography system and a selection of prepacked disposable columns. Thin-layer chromatography was performed using Merck 0.25 mm silica layer foil-backed plates.

NMR spectra were recorded on Bruker DPX-300, DPX-400, and AV-400 spectrometers. ^1H and ^{13}C spectra were referenced internally using residual protio solvent resonances relative to tetramethylsilane (δ 0 ppm). Proton and carbon NMR assignments were routinely confirmed by $^1H-^1H$ (COSY) or $^1H-^{13}C$ (HMQC) experiments. Infrared spectra were obtained directly using an Avatar 320 FTIR instrument. EI mass spectra were obtained on a VG Autospec mass spectrometer. Elemental analyses were performed by Warwick Analytical Services. Low percentage C values were obtained in the elemental analysis of a few of the organometallic complexes, despite their apparent purity as judged by ^1H NMR (see the Supporting Information). This is attributed to the partial formation of metal carbides in the combustion process, as frequently observed with systems of this type.[34]

[Cp*ZrL^{1}Cl$_2$]. H**L^1** (153 mg, 0.56 mmol) and NaH (54 mg, 2.22 mmol) were cooled to −78 °C in a Schlenk vessel and dissolved in THF (10 cm^3). The yellow mixture was warmed to room temperature and stirred for 15 h. The mixture was filtered onto a solution of Cp*$ZrCl_3$ (185 mg, 0.56 mmol) in THF (10 cm^3) at −78 °C. The resulting yellow solution was stirred for 24 h, affording a fine white precipitate. The solvent was removed under vacuum, and the crude solid was dissolved in toluene (10 cm^3) and this solution filtered. The solvent was removed under vacuum, leaving an off-white solid, which was crystallized from diethyl ether and dried thoroughly in vacuo. Desolvation occurred during this latter process, and only traces of solvent were detected by NMR spectroscopy. Yield: 178 mg, 56%. Anal. Calcd for $C_{27}H_{39}Cl_2NO_2Zr$: C, 56.72; H, 6.88; N, 2.45. Found: C, 55.88; H, 6.90; N, 2.59. ^1H NMR (400 MHz, 298 K, C_6D_6): δ 7.83 (d, $^4J_{HH}$ = 3 Hz, 1H, Ar *H*), 7.72 (d, $^4J_{HH}$ = 3 Hz, 1H, Ar *H*), 3.70−3.85 (m, 1H, NC*H*$_2$), 3.48−3.55 (m, 1H, OC*H*$_2$), 3.36−3.46 (m, 2H, NC*H*$_2$C*H*$_2$O), 1.90 (s, 15H, *Cp**), 1.66 (s, 9H, C(C*H*$_3$)$_3$), 1.26 (s, 9H, C(C*H*$_3$)$_3$) ppm. $^{13}C\{^1H\}$ NMR (100 MHz, 298 K, C_6D_6): δ 169.2 (N=*C*O), 162.1, 141.3, 140.2, 130.7, 125.2, 123.6 (Ar C), 112.1 (*C*$_5$Me$_5$), 67.1 (O*C*H$_2$), 57.0 (N*C*H$_2$), 35.8, 34.5 (*C*(CH$_3$), 31.5, 30.3 (C(*C*H$_3$), 12.1 (C$_5$*Me*$_5$). MS (EI): *m*/*z* 571 [M^+].

[Cp*ZrL^{2}Cl$_2$]. The procedure was as for Cp*Zr**L^1**Cl$_2$, using H**L^2**. Yield: 321 mg, 58%. Anal. Calcd for $C_{29}H_{43}Cl_2NO_2Zr$: C, 58.07; H, 7.23; N, 2.34. Found: C, 57.97; H, 7.24; N, 1.87. ^1H NMR (400 MHz, 298 K, C_6D_6): δ 8.00 (1H, d, Ar *H*, $^4J_{HH}$ = 3 Hz), 7.71 (1H, d, Ar *H*, $^4J_{HH}$ = 3 Hz), 3.49 (1H, d, OC*H*$_2$, $^2J_{HH}$ = 8 Hz), 3.35 (1H, d, OC*H*$_2$, $^2J_{HH}$ = 8 Hz), 1.90 (15H, s, C$_5$*Me*$_5$), 1.64 (9H, s, *t Bu*), 1.49 (3H, s, NC*Me*$_2$), 1.28 (9H, s, *t Bu*), 1.04 (3H, s, NC*Me*$_2$) ppm. $^{13}C\{^1H\}$ NMR (100 MHz, 298 K, C_6D_6): δ 169.2 (N=*C*O), 162.0, 141.8, 140.3, 130.6, 126.2, 123.7 (Ar C), 113.3 (*C*$_5$Me$_5$), 78.7 (O*C*H$_2$), 71.5 (N*C*Me$_2$), 35.7, 34.6 (*C*(CH$_3$)$_3$), 31.5, 30.1 (C(*C*H$_3$)$_3$), 27.7, 24.9 (NC*Me*$_2$), 12.6 (C$_5$*Me*$_5$) ppm. MS (EI): *m*/*z* 598 [M^+].

[Cp*ZrL^{3}Cl$_2$]. H**L^3** (225 mg, 0.90 mmol) and NaH (87 mg, 3.63 mmol) were cooled to −78 °C in a Schlenk vessel and dissolved in THF (10 cm^3). The yellow mixture was warmed to room temperature and stirred for 15 h. The mixture was filtered onto a solution of Cp*$ZrCl_3$ (300 mg, 0.90 mmol) in THF (10 cm^3) at −78 °C. The resulting yellow solution was stirred for 24 h, affording a fine white precipitate. The solvent was removed under vacuum, and the crude solid was dissolved in dichloromethane (10 cm^3) and the solution filtered. The solvent was removed under vacuum, leaving an off-white solid, which was washed with diethyl ether, yielding [Cp*Zr**L^3**Cl$_2$] as a white solid. Yield: 309 mg, 63%. Anal. Calcd for $C_{24}H_{33}Cl_2NO_3Zr$: C, 52.83; H, 6.10; N, 2.57. Found: C, 50.85; H, 6.01; N, 2.35. ^1H NMR (400 MHz, 298 K, CD_2Cl_2): δ 7.12 (2H, s, Ar *H*), 4.58−4.64 (1H, m, OC*H*$_2$), 4.22−4.44 (2H, m OC*H*$_2$C*H*$_2$N), 3.96−4.04 (1H, m, C*H*$_2$N), 3.73 (3H, s, O*Me*), 1.95 (15H, s, C$_5$*Me*$_5$), 1.37 (9H, s, *t Bu*) ppm. $^{13}C\{^1H\}$ NMR (100 MHz, 298 K, CD_2Cl_2): δ 169.3 (N=*C*O), 158.6, 152.2, 141.9, 125.8, 122.8 (Ar C), 111.7 (*C*$_5$Me$_5$), 107.8 (Ar C), 68.2 (O*C*H$_2$), 57.2 (N*C*H$_2$), 55.7 (O*Me*), 35.3 (*C*(CH$_3$)$_3$), 29.7 (C(*C*H$_3$)$_3$), 11.9 (C$_5$*Me*$_5$) ppm. MS (EI): *m*/*z* 545 [M^+].

[Cp*ZrL^{4}Cl$_2$]. The procedure was as for Cp*Zr**L^1**Cl$_2$, using H**L^4**. Yield: 332 mg, 68%. Anal. Calcd for $C_{26}H_{37}Cl_2NO_3Zr$: C, 54.43; H, 6.53; N, 2.44. Found: C, 54.70; H, 6.59; N, 2.81. ^1H NMR (400 MHz, 298 K, C_6D_6): δ 7.32 (1H, d, Ar *H*, $^4J_{HH}$ = 8 Hz), 7.31 (1H, d, Ar *H*, $^4J_{HH}$ = 8 Hz), 3.48 (1H, d, OC*H*$_2$, $^2J_{HH}$ = 8 Hz), 3.40 (3H, s, O*Me*), 3.34 (1H, d, OC*H*$_2$, $^2J_{HH}$ = 8 Hz), 1.91 (15H, s, C$_5$*Me*$_5$), 1.54 (9H, s, *t Bu*), 1.50 (3H, s, NC*Me*$_2$), 1.04 (3H, s, NC*Me*$_2$) ppm. $^{13}C\{^1H\}$ NMR (100 MHz, 298 K, CD_2Cl_2) δ 169.3 (N=*C*O), 159.2, 152.6, 142.4, 126.2, 122.9 (Ar C), 113.3 (*C*$_5$Me$_5$), 108.2 (Ar C), 78.7 (O*C*H$_2$), 71.6 (N*C*Me$_2$), 55.2 (O*Me*), 35.6 (*C*(CH$_3$)$_3$), 29.9 (C(*C*H$_3$)$_3$), 27.6, 24.9 (NC*Me*$_2$), 12.6 (C$_5$*Me*$_5$) ppm. MS (EI): *m*/*z* 571 [M^+].

[Cp*HfL^{1}Cl$_2$]. The procedure was as for [Cp*Zr**L^1**Cl$_2$], using Cp*$HfCl_3$. Yield: 298 mg, 53%. Anal. Calcd for $C_{27}H_{39}Cl_2NO_2Hf$: C, 49.21; H, 5.97; N, 2.13. Found: C, 48.77; H, 5.93; N, 2.08. ^1H NMR (400 MHz, 298 K, d_8-toluene): δ 7.74 (1H, d, $^4J_{HH}$ = 3 Hz, Ar *H*), 7.66 (1H, d, $^4J_{HH}$ = 3 Hz, Ar *H*), 3.60−3.70 (1H, m, C*H*$_2$), 3.28−3.50 (3H, m, C*H*$_2$C*H*$_2$), 1.88 (15H, s, *Cp**), 1.57 (9H, s, C(C*H*$_3$)$_3$), 1.22 (9H, s, C(C*H*$_3$)$_3$). $^{13}C\{^1H\}$ NMR (100 MHz, 298 K, d_8-toluene): δ 169.3 (N=*C*O), 162.3, 141.1, 140.8, 131.0, 123.4, 123.0, (Ar C), 111.8 (*C*$_5$Me$_5$), 67.3 (O*C*H$_2$), 56.8 (N*C*H$_2$), 35.7, 34.5 (*C*(CH$_3$), 31.5, 30.3 (C(*C*H$_3$)), 11.8 (C$_5$*Me*$_5$). MS (EI): *m*/*z* 659 [M^+].

(33) (a) Pennington, D. A.; Clegg, W.; Coles, S. J.; Harrington, R. W.; Hursthouse, M. B.; Hughes, D. L.; Light, M. E.; Schormann, M.; Bochmann, M.; Lancaster, S. J. *Dalton Trans.* **2005**, 561. (b) Pennington, D. A.; Hughes, D. L.; Bochmann, M.; Lancaster, S. J. *Dalton Trans.* **2003**, 3480. (c) Makio, H.; Fujita, T. *Macromol. Symp.* **2004**, *213*, 221. (d) Bryliakov, K. P.; Kravtsov, E. A.; Pennington, D. A.; Lancaster, S. J.; Bochmann, M.; Brintzinger, H. H.; Talsi, E. P. *Organometallics* **2005**, *24*, 5660.

(34) Carpenetti, D. W.; Kloppenburg, L.; Kupec, J. T.; Petersen, J. L. *Organometallics* **1996**, *15*, 1572.

[Cp*HfL²Cl₂]. The procedure was as for [Cp*Zr**L¹**Cl₂], using Cp*HfCl₃ and H**L²**. Yield: 305 mg, 58%. Anal. Calcd for $C_{29}H_{43}Cl_2NO_2Hf\cdot 0.1Et_2O$: C, 50.85; H, 6.39; N, 2.02. Found: C, 49.87; H, 6.09; N, 1.92. ^{1}H NMR (400 MHz, 298 K, CD_2Cl_2): δ 7.66 (1H, d, Ar *H*, $^4J_{HH}$ = 3 Hz), 7.54 (1H, d, Ar *H*, $^4J_{HH}$ = 3 Hz), 4.27 (1H, d, OC*H*$_2$, $^2J_{HH}$ = 8 Hz), 3.99 (1H, d, OC*H*$_2$, $^2J_{HH}$ = 8 Hz), 1.92 (15H, s, C_5*Me*$_5$), 1.75 (3H, s, NC*Me*$_2$), 1.38 (9H, s, ^{t}*Bu*), 1.35 (3H, s, NC*Me*$_2$), 1.26 (9H, s, ^{t}*Bu*) ppm. ^{13}C{^{1}H} NMR (100 MHz, 298 K, CD_2Cl_2): δ 169.2 (N=*C*O), 142.0, 140.0, 132.4, 131.1, 124.4, 123.9 (Ar C), 112.9 (*C*$_5$Me$_5$), 79.6 (O*C*H$_2$), 72.0 (N*C*Me$_2$), 35.4, 34.7 (*C*(CH$_3$)$_3$), 31.5, 29.9 (C(*C*H$_3$)$_3$), 28.1, 25.1 (NC*Me*$_2$), 12.3 (C$_5$*Me*$_5$) ppm. MS (EI): *m*/*z* 687 [M$^+$].

[CpTiL¹Cl₂]. H**L¹** (300 mg, 1.09 mmol) and NaH (105 mg, 4.38 mmol) were cooled to −78 °C in a Schlenk vessel, and dissolved in THF (10 cm^3). The yellow mixture was warmed to room temperature, and left stirring for 15 h. The mixture was filtered onto a solution of $CpTiCl_3$ (239 mg, 1.09 mmol) in THF (10 cm^3) at −78 °C. The resulting red solution was stirred for 24 h, affording a fine white precipitate. The solvent was removed under vacuum, and the crude solid was dissolved in toluene (10 cm^3) and filtered. The solvent was removed under vacuum, leaving a dark red solid, which was purified by recrystallization from dichloromethane. Yield: 217 mg, 43%. Anal. Calcd for $C_{22}H_{29}Cl_2NO_2Ti$: C, 57.66; H, 6.38; N, 3.06. Found: C, 57.33; H, 6.32; N, 3.06. ^{1}H NMR (400 MHz, 298 K, CD_2Cl_2): δ 7.69 (1H, d, Ar *H*, $^4J_{HH}$ = 3 Hz), 7.61 (1H, d, Ar *H*, $^4J_{HH}$ = 3 Hz), 6.50 (5H, s, C_5H_5), 4.54−4.60 (3H, m, OC*H*$_2$C*H*$_2$N), 4.10−4.15 (1H, m, C*H*$_2$N), 1.39 (9H, s, ^{t}*Bu*), 1.28 (9H, s, ^{t}*Bu*) ppm. ^{13}C{^{1}H} NMR (100 MHz, 298 K, CD_2Cl_2): δ 167.2 (N=*C*O), 165.7, 144.4, 138.0, 130.9, 123.1, 122.1 (Ar *C*), 112.4 (*C*$_5$H$_5$), 68.5 (O*C*H$_2$), 59.2 (N*C*Me$_2$), 35.5, 35.0 (*C*(CH$_3$)$_3$), 31.5, 29.9 (C(*C*H$_3$)$_3$) ppm. MS (EI): *m*/*z* 458 [M$^+$].

[Cp*ZrL¹Me₂]. H**L¹** (280 mg, 1.02 mmol) and Cp^*ZrMe_3 (276 mg, 1.02 mmol) were charged into a Schlenk vessel and dissolved in toluene (10 cm^3). Gas was observed almost instantaneously, and the mixture was stirred for 15 h. The solvent was removed, and the crude off-white solid was purified by recrystallization from pentane. Yield: 221 mg, 41%. Anal. Calcd. for $C_{29}H_{45}NO_2Zr$: C 65.61; H 8.54; N 2.64. Found: C 64.61; H 8.37; N 2.70. ^{1}H NMR (400 MHz, 298 K, d_8-toluene): δ 7.89 (1H, d, $^4J_{HH}$ = 3 Hz, Ar *H*), 7.66 (1H, d, $^4J_{HH}$ = 3 Hz, Ar *H*), 3.51−3.57 (1H, m, OC*H*$_2$), 3.36−3.44 (1H, m, OC*H*$_2$), 3.24−3.32 (1H, m, NC*H*$_2$), 3.07−3.14 (1H, m, NC*H*$_2$), 1.77 (15H, s, *Cp**), 1.54 (9H, s, C(*Me*)$_3$), 1.27 (9H, s, C(*Me*)$_3$), 0.41 (3H, s, Zr*Me*), 0.03 (3H, s, Zr*Me*). ^{13}C{^{1}H} NMR (100 MHz, 298 K, d_8-toluene): δ 167.4 (N=*C*O), 162.0, 138.4, 136.1, 128.5, 123.7, 117.7 (Ar C), 110.2 (*C*$_5$Me$_5$), 65.1 (O*C*H$_2$), 53.9 (N*C*H$_2$), 39.4, 37.5 (Zr*Me*), 34.3, 33.1 (*C*(Me)$_3$), 30.3, 28.8 (C(*Me*)$_3$), 9.9 (C$_5$*Me*$_5$). MS (EI): *m*/*z* 514 [M$^+$ − Me].

[Cp*ZrL²Me₂]. The procedure was as for [Cp*Zr**L¹**Me$_2$], using H**L²**. Yield: 145 mg, 48%. Anal. Calcd for $C_{31}H_{49}NO_2Zr$: C, 66.61; H, 8.84; N, 2.51. Found: C, 66.52; H, 8.99; N, 2.69. ^{1}H NMR (400 MHz, 298 K, d_8-toluene): δ 7.98 (1H, d, $^4J_{HH}$ = 3 Hz, Ar *H*), 7.63 (1H, d, $^4J_{HH}$ = 3 Hz, Ar *H*), 3.47 (2H, d, $^2J_{HH}$ = 8 Hz, OC*H*$_2$), 3.28 (2H, d, $^2J_{HH}$ = 8 Hz, OC*H*$_2$), 1.79 (15H, s, *Cp**), 1.50 (9H, s, C(*Me*)$_3$), 1.26 (9H, s, C(*Me*)$_3$), 1.15 (3H, s, NC*Me*), 0.92 (3H, s, NC*Me*), 0.59 (3H, s, Zr*Me*), 0.25 (3H, s, Zr*Me*). ^{13}C{^{1}H} NMR (100 MHz, 298 K, d_8-toluene): δ 168.5 (N=*C*O), 162.7, 139.4, 128.8, 124.0, 120.0 (Ar C), 112.6 (*C*$_5$Me$_5$), 78.3 (O*C*H$_2$), 70.1 (N*C*Me$_2$), 45.1, 40.0 (Zr*Me*), 35.6, 34.5 (*C*(Me)$_3$), 31.6, 30.1 (C(*Me*)$_3$), 27.8, 25.2 (NC*Me*), 11.8 (C$_5$*Me*$_5$). MS (EI): *m*/*z* 542 [M$^+$ − Me].

[Cp*HfL¹Me₂]. The procedure was as for [Cp*Zr**L¹**Me$_2$], using Cp^*HfMe_3. Yield: 353 mg, 66%. Anal. Calcd for $C_{29}H_{45}NO_2Hf$: C, 56.35; H, 7.34; N, 2.27. Found: C, 55.99; H, 7.22; N, 1.95. ^{1}H NMR (400 MHz, 298 K, d_8-toluene): δ 7.87 (1H, d, $^4J_{HH}$ = 3 Hz, Ar *H*), 7.67 (1H, d, $^4J_{HH}$ = 3 Hz, Ar *H*), 3.50−3.55 (1H, m, OC*H*$_2$), 3.37−3.44 (1H, m, OC*H*$_2$), 3.21−3.30 (1H, m, NC*H*$_2$), 3.10−3.17 (1H, m, NC*H*$_2$), 1.80 (15H, s, *Cp**), 1.55 (9H, s, C(*Me*)$_3$), 1.26 (9H, s, C(*Me*)$_3$), 0.25 (3H, s, Hf*Me*), −0.21 (3H, s, Hf*Me*). ^{13}C{^{1}H} NMR (100 MHz, 298 K, d_8-toluene): δ 168.4 (N=*C*O), 163.4, 140.2, 139.2, 130.0, 123.4, 118.1 (Ar *C*), 111.3 (*C*$_5$Me$_5$), 66.7 (O*C*H$_2$), 55.1 (N*C*H$_2$), 45.2, 43.8 (Hf*Me*), 35.7, 34.5 (*C*(Me)$_3$), 31.6, 30.2 (C(*Me*)$_3$), 11.1 (C$_5$*Me*$_5$). MS (EI): *m*/*z* 604 [M$^+$].

[Cp*HfL²Me₂]. The procedure was as for [Cp*Zr**L¹**Me$_2$], using H**L²** and Cp^*HfMe_3. Yield: 222 mg, 59%. Anal. Calcd for $C_{31}H_{49}NO_2Hf$: C, 57.62; H, 7.64; N, 2.17. Found: C, 56.75; H, 7.56; N, 2.30. ^{1}H NMR (400 MHz, 298 K, d_8-toluene): δ 8.02 (1H, d, $^4J_{HH}$ = 3 Hz, Ar *H*), 7.70 (1H, d, $^4J_{HH}$ = 3 Hz, Ar *H*), 3.52 (2H, d, $^2J_{HH}$ = 8 Hz, OC*H*$_2$), 3.36 (2H, d, $^2J_{HH}$ = 8 Hz, OC*H*$_2$), 1.88 (15H, s, *Cp**), 1.57 (9H, s, C(*Me*)$_3$), 1.32 (9H, s, C(*Me*)$_3$), 1.24 (3H, s, NC*Me*), 0.96 (3H, s, NC*Me*), 0.43 (3H, s, Hf*Me*), 0.14 (3H, s, Hf*Me*). ^{13}C{^{1}H} NMR (100 MHz, 298 K, d_8-toluene): δ 162.6 (N=*C*O), 139.9, 139.6, 129.1, 123.8, 119.0, 112.6 (Ar *C*), 78.6 (O*C*H$_2$), 70.2 (N*C*Me$_2$), 48.8, 46.3 (Hf*Me*), 35.6, 34.5 (*C*(Me)$_3$), 31.6, 30.1 (C(*Me*)$_3$), 27.8, 25.1 (NC*Me*), 11.7 (*Cp**). MS (EI): *m*/*z* 632 [M$^+$ − Me].

Typical Polymerization. A solution of ^{i}Bu$_3$Al in toluene (0.1 M, 6 cm^3) was added to toluene (100 cm^3) under an atmosphere of argon. The vessel was evacuated and heated to the desired temperature. A constant pressure supply of ethylene (1.2 bar) was introduced, and the system was allowed to equilibrate. During this time, a catalyst solution was prepared by dissolving the precatalyst (1−6 mg) and $[PhNMe_2H]^+[B(C_6F_5)_4]^-$ (9 mg) in toluene (5 cm^3). The catalyst solution was injected, and the gas flow and temperature (±0.5 °C) were monitored. After 1 h, the ethylene atmosphere was then replaced with argon and 5% HCl in methanol (2 × 10 cm^3) was then added to the slurry. The slurry was then poured into methanol (500 cm^3) with stirring, and the polymer was allowed to precipitate for approximately 1 h. The polymer was isolated by filtration and washed with 5% HCl in methanol (50 cm^3) and methanol (2 × 50 cm^3). The polymer was then dried in a vacuum oven at 60 °C until constant weight was achieved.

Crystallography. Crystals of [Cp*Zr**L¹**Cl$_2$], [Cp*Zr**L²**Cl$_2$], and [Cp*Hf**L¹**Cl$_2$] were obtained as colorless blocks by cooling a concentrated solution in diethyl ether to −30 °C. Crystals of [Cp*Zr**L¹**Me$_2$] were similarly obtained from a concentrated solution in pentane. Crystals were coated in an inert oil prior to transfer to a cold nitrogen gas stream on a Bruker-AXS SMART three-circle CCD area detector diffractometer system equipped with Mo Kα radiation (λ = 0.710 73 Å). Data were collected using narrow (0.3° in ω) frame exposures. Intensities were corrected semiempirically for absorption, on the basis of symmetry-equivalent and repeated reflections (SADABS). The structures were solved by direct methods (SHELXS) with additional light atoms found by Fourier methods. All non-hydrogen atoms were refined anisotropically. All H atoms were constrained with a riding model; *U*(H) was set at 1.2 (1.5 for methyl hydrogen atoms as applicable) times U_{eq} for the parent atom. Programs used were Bruker AXS SMART (control), SAINT (integration), and SHELXTL for structure solution, refinement, and molecular graphics.

The crystal structures of [Cp*Zr**L¹**Cl$_2$] and [Cp*Hf**L¹**Cl$_2$] are isomorphous and contain diffuse electron density modeled as a molecule of diethyl ether from the crystallization. This was found to reside in a position of higher symmetry than is possible for diethyl ether; therefore, it was modeled as two molecules at 25% occupancy related by inversion symmetry at the oxygen atom (O103). No hydrogens were added for the disordered diethyl ether molecules but were included in the formula for calculation of the density.

The crystal chosen of [Cp*Zr**L²**Cl$_2$] was chiral with a small twin component BASF refined to 0.079(72).

Computations. All geometry optimizations were performed with the DMol^3 density functional theory (DFT) code[35] as implemented in the MaterialsStudio (versions 3.2 and 4.0) program package of

(35) (a) Delley, B. *J. Chem. Phys.* **1990**, *92*, 508. (b) Delley, B. *J. Phys. Chem.* **1996**, *100*, 6107. (c) Delley, B. *J. Chem. Phys.* **2000**, *113*, 7756.

Accelrys Inc. DMol[3] utilizes a basis set of numeric atomic functions, which are exact solutions to the Kohn−Sham equations for the atoms.[36] These basis sets are generally more complete than a comparable set of linearly independent Gaussian functions and have been demonstrated to have small basis set superposition errors.[36] In the present study a polarized split valence basis set, termed the double numeric polarized (DNP) basis set, has been used, containing a p-polarization function for H and d-polarization functions for other atoms. The DNP basis set was chosen because it is equivalent in quality and size to the Gaussian 6-31G** split-valence double-ζ plus polarization basis set, generally accepted as the standard basis set in quantum chemistry. All geometry optimizations employed highly efficient delocalized internal coordinates.[37] The use of delocalized coordinates significantly reduces the number of geometry optimization iterations needed to optimize larger molecules compared to the use of traditional Cartesian coordinates.

The generalized gradient approximation (GGA) functional by Becke and Perdew (BP)[38] was used for all geometry optimizations. The convergence criteria for these optimizations consisted of threshold values of 2×10^{-5} hartree, 0.004 hartree Å^{-1}, and 0.005 Å for energy, gradient, and displacement convergence, respectively, while a self-consistent field (SCF) density convergence threshold value of 1×10^{-5} was specified.

Preliminary transition state geometries were obtained by the integrated linear synchronous transit/quadratic synchronous transit (LST/QST) algorithm[39] available in MaterialsStudio. These preliminary structures were then subjected to full TS optimizations using an eigenvector following algorithm. All transition structure geometries exhibited only one imaginary frequency in the reaction coordinate. All calculated reaction energies were derived from the total electronic energies of the geometries after optimization.

Acknowledgment. PS thanks EPSRC and BP Chemicals/INEOS for support.

Supporting Information Available: CIF files for the molecular structure determinations and structure files for the computed species in Table 5. This material is available free of charge via the Internet at http://pubs.acs.org.

OM060687H

(36) (a) Delley, B. In *Density Functional Theory: A Tool for Chemistry*; (b) Seminario, J. M., Politzer, P., Eds.; Elsevier: Amsterdam, The Netherlands, 1995.

(37) Andzelm, J.; King-Smith, R. D.; Fitzgerald, G. *Chem. Phys. Lett.* **2001**, *335*, 321.

(38) (a) Becke, A. D. *J. Chem. Phys.* **1988**, *88*, 2547; (b) Perdew, J. P.; Wang, Y. *Phys. Rev. B* **1992**, *45*, 13244.

(39) Govind, N.; Petersen, M.; Fitzgerald, G.; King-Smith, D.; Andzelm, J. *Comput. Mater. Sci.* **2003**, *28*, 250.